4 A mathematical model for solidification of binary eutectic system including relaxation time

4.1 Introduction

The solidification of eutectic alloy is an interesting area of research in metallurgy and material science due to their anisotropic properties. In general, the solidification of pure substance changes phase isothermally and the smooth interface exist between the phases. The solidification of an alloy is different than that of pure substance and not solidify isothermally. When the liquid starts to freeze at liquidus temperature and the liquid freezes partially and gradually until the temperature drops to eutectic temperature therefore, the remaining liquid freezes isothermally at that temperature. In this case, the system contains two phase (solid-liquid) region, often referred to as the mushy region. In this region the latent heat associated with phase change is evolved. The melting/solidification of multi-component occur in a range of temperature while in single component, the phase change occur at unique temperature.

In last few decades, the several mathematical models have been studied in the area of solidification of binary systems such as NH_4Cl-H_2O, $NaCl-H_2O$, $Pb-Sn$, $Al-Cu$ (Viskanta (1988), Braga and Viskanta (1990), Zeng and Faghri (1994a,b)). Tien and Geiger (1967) studied the one dimensional solidification of a binary eutectic system in a semi-infinite medium when surface temperature is constant. Further, Tien and Geiger (1968) investigated unidirectional solidification of binary eutectic system when surface temperature is time dependent. Cho and Sunderland (1969)

proposed an exact solution for a semi-infinite body where the change of phases occurred over an extended freezing temperature range and presented an approximate solution for finite slab by using the heat-balance integral technique. An exact solution for freezing in a cylindrical symmetry in infinite medium was given by Özisik and Uzzell (1979). An analytical solution was given by Chakraborty and Dutta (2002) for conduction dominated unidirectional solidification of binary mixture. A mathematical model has been proposed for solute redistribution in mushy zone during solidification of $Al - Cu$ alloys by Diao and Tsai (1993). In this model, they have examined the effect of shrinkage-induced fluid flow and solute diffusion on the formation of macro-segregation. An approximate closed form analytical solution of the de-sublimation problem in a porous medium has been proposed by Rai and Rai (1995). A semi-exact solution for solidification of a binary solution on a cold isothermal surface below eutectic temperature was given by Shi and Zhang (2009). Several other mathematical models for solidification of alloys have been studied by Rai and Singh (1998); Voller and Prakash (1987a); Voller (1987b); Voller and Brent (1990); Voller *et al.* (2004); Voller (2008) and many others.

Most of the numerical technique have been employed by Crank (1984) to solve the solidification of binary alloy. The finite-difference method is used by Clyne (1982) in the modelling of directional solidification of a metallic alloys. Voller (1989) proposed the mushy heat balance integral method in conjunction with the enthalpy model to analyze the unidirectional solidification of a binary eutectic alloy. Swaminathan (1992) used a general implicit source-based enthalpy method to solve two-dimensional solidification problems with a mushy zone. A thermal model for binary solution ($NH_4Cl - H_2O$) has been presented by Zhang and Faghri (1998). A numerical simulation for two-dimensional moving boundary problems with mushy zone was studied by Cheng (1999). A finite element method has been used by Skrzypcza and krzypczak (2012) for solidification process of pure metals. Recently, Yadav *et al.* (2014) used wavelet Galerkin and wavelet collection method in two phase moving boundary problems. Further, Yadav *et al.* (2014) used finite element Legendre wavelet Galerkin method to solve inward solidification of moving boundary problems. Most of the work in phase change problems are based on classical Fourier

law of heat conduction (Carslaw and Jaegar (1959)) and defined as:

$$q(r,t) = -K\frac{\partial T(r,t)}{\partial r}. \tag{4.1}$$

Now a days, the great attention has been focused on energy transport in micro-scale level. In this case the heat is found to propagate at a finite speed. In order to account the phenomena involving finite speed of propagation, the classical Fourier law of heat conduction has been modified by Cattaneo (1958) and Vernotte (1961) (CV constitution) in the form

$$q(r,t+\tau_q) = -K\frac{\partial T(r,t)}{\partial r}, \tag{4.2}$$

where q is heat flux, T is temperature, K is thermal conductivity of material and τ_q is relaxation time. The constitutive relation defined in Eq. (4.2) is called single-phase-lagging (SPL) heat conduction model. Using the Taylors series expansion the CV constitution relation of Eq. (4.2) reduces in the form of

$$q(r,t) + \tau_q\frac{\partial q(r,t)}{\partial t} = -K\frac{\partial T(r,t)}{\partial r}. \tag{4.3}$$

The application of hyperbolic heat conduction are presented by Han Taw and Jae Yuh (1989), Kim *et al.* (1999), Al-Nimr (2001), Yang (2009) and Ramadan (2009) in different configuration.

In this chapter, we have considered the time relaxation model for solidification of binary eutectic system. The binary eutectic system which is cooled by flat probe whose temperature is decreased with time. The solidification process has been occurred in three stages. (i) In first stage, the melt is cooled up to liquidus temperature T_l, (ii) when melt is cooled up to freezing temperature T_f. In this stage mushy-liquid region is formed. (iii) when surface temperature of flat probe is continuously decreasing, the freezing start and the solid region, mushy region and liquid region are formed. In each phase, the relaxation time is considered. In this process, the non Fourier heat is conducted in a binary system when surface is cooled. The internal heat generation A in the mushy region is defined as:

$$A = \rho L\frac{df_s}{dt}, \tag{4.4}$$

where f_s is solid fraction present in mushy region.

The solid fraction f_s in the mushy region depends on various physical parameters, such as the temperature of the mushy region and the distance of the mushy region. An exact mathematical expression for the solid fraction in the mushy region cannot be given and in its absence some approximate mathematical models are proposed. Two such models have been considered by Gupta (2000), Gupta (2003) for the numerical solution of the problem and defined as:

$$f_S = \frac{f_{su}\left(s_2(t) - r\right) - f_{su_1}\left(s_1(t) - r\right)}{s_2(t) - s_1(t)}, \tag{4.5}$$

$$f_S = \frac{f_{su}\left(T_l - T_2\right) - f_{su_1}\left(T_f - T_2\right)}{T_l - T_f}, \tag{4.6}$$

where f_{su} and f_{su_1} are solid fractions present at solid-mushy and liquid-mushy boundaries respectively, f_s is the solid fraction present in the mushy region. In generally, f_{su} taken as unity but in case of eutectic, it can be taken less than unity ($0 < f_{su} < 1$) and at the liquid-mushy boundary, $f_{su_1} = 0$ is considered. In this paper we considered that the solid fraction is also present at the liquid-mushy boundary, i.e. $f_{su_1} \neq 0$. Then, we have an implicit moving boundary condition which is a difficult task for the numerical solution.

To solve this model we have established the Legendre Wavelets spectral Galerkin method. The theory of spectral methods was described in several books such as Gottlieb (1977), Boyd (2000), Canuto (2006). In this method, we have developed the new approach of spectral Galerkin method with Legendre wavelets basis functions. Further, We have proved the well-posedness of model and stability analysis of method.

4.2 Formulation of Mathematical Model

Consider a binary eutectic system initially at uniform temperature T_i which is greater than liquidus temperature T_l of a melt. At time $t = 0$, the melt is cooled by a flat probe whose temperature decreases with time. The cooling start and the whole process of cooling is composed in three stages. In stage I, the probe surface is cooled at a constant rate g, from the initial temperature T_i to liquidus temperature

T_l. Further, in Stage II, the flat probe is continuously cooled at constant rate g from the liquidus temperature T_l to freezing temperature T_f. During this stage the mushy region and liquid region simultaneously co-exist. In stage III, when the temperature of flat probe is continuously decreased with time the solidification starts from the origin and propagates in the positive r- direction. In this stage solid region, mushy region and liquid region are formed. The physical properties (thermal conductivity, specific heat) of each phases are assumed to be constant but differ for different phases. The density of each region is equal and constant i.e. $\rho_1 = \rho_2 = \rho$ and the volumetric change in entire solidification process is negligible. The mathematical model for binary eutectic system, by using non- Fourier heat conduction law is described as follows:

Stage I

$$\frac{\partial T_3}{\partial t_1} + \tau_{q_3} \frac{\partial^2 T_3}{\partial t_1^2} = a_3 \frac{\partial^2 T_3}{\partial r^2}, 0 < r < l, t_1 > 0. \tag{4.7}$$

The associated initial and boundary conditions are

$$T_3(r, 0) = T_i, \frac{\partial T_3(r, 0)}{\partial t_1} = g_1, \tag{4.8}$$

$$T_3(0, t_1) = T_i - g t_1, \frac{\partial T_3(l, t_1)}{\partial r} = 0. \tag{4.9}$$

Stage II

$$\frac{\partial T_2}{\partial t_2} + \tau_{q_2} \frac{\partial^2 T_2}{\partial t_2^2} = a_2 \frac{\partial^2 T_2}{\partial r^2} + \frac{a_2 A}{k_2}, 0 < r < s_2(t_2), t_2 > t_1, \tag{4.10}$$

$$\frac{\partial T_3}{\partial t_2} = a_3 \frac{\partial^2 T_3}{\partial r^2}, s_2(t_2) < r < l. \tag{4.11}$$

The associated initial and boundary conditions are

$$T_2(r, t_1^*) = T_3(r, t_1^*), \frac{\partial T_2(r, t_1^*)}{\partial t_2} = g_1, \tag{4.12}$$

$$T_2(0, t_2) = T_l - g t_2. \tag{4.13}$$

The interface conditions are

$$T_2(s_2(t_2), t_2) = T_3(s_2(t_2), t_2) = T_l, \tag{4.14}$$

$$K_2 \frac{\partial T_2(r, t_2)}{\partial r} - K_3 \frac{\partial T_3(r, t_2)}{\partial r} = \rho L f_{su_1} \frac{\partial r}{\partial t_2}, r = s_2(t_2), \tag{4.15}$$

$$\frac{\partial T_3(l,t_2)}{\partial r} = 0, \tag{4.16}$$
$$t_1^* = \frac{T_i - T_l}{g},$$
$$t_2 = t_1 - t_1^*.$$

Stage III

$$\frac{\partial T_1}{\partial t_3} + \tau_{q_1}\frac{\partial^2 T_1}{\partial t_3^2} = a_1\frac{\partial^2 T_1}{\partial r^2}, 0 < r < s_1(t_3), t_3 > t_2, \tag{4.17}$$

$$\frac{\partial T_2}{\partial t_3} = a_2\frac{\partial^2 T_2}{\partial r^2} + \frac{a_2 A}{k_2}, s_1(t_3) < r < s_2(t_3), \tag{4.18}$$

$$\frac{\partial T_3}{\partial t_3} = a_3\frac{\partial^2 T_3}{\partial r^2}, s_2(t_3) < r < l. \tag{4.19}$$

The associated initial and boundary conditions are

$$T_1(r,t_2^*) = T_2(r,t_2^*) = T_3(r,t_2^*), \frac{\partial T_1(r,t_2^*)}{\partial t_3} = g_1, \tag{4.20}$$

$$T_1(0,t_3) = T_f - gt_3. \tag{4.21}$$

The interface conditions are

$$T_1(s_1(t_3),t_3) = T_2(s_1(t_3),t_3) = T_f, \tag{4.22}$$

$$T_2(s_2(t_3),t_3) = T_3(s_2(t_3),t_3) = T_l, \tag{4.23}$$

$$K_1\frac{\partial T_1(r,t_3)}{\partial r} - K_2\frac{\partial T_2(r,t_3)}{\partial r} = \rho L(1-f_{su})\frac{\partial r}{\partial t_3}, r = s_1(t_3), \tag{4.24}$$

$$K_2\frac{\partial T_2(r,t_3)}{\partial r} - K_3\frac{\partial T_3(r,t_3)}{\partial r} = \rho L f_{su_1}\frac{\partial r}{\partial t_3}, r = s_2(t_3), \tag{4.25}$$

$$\frac{\partial T_3(l,t_3)}{\partial r} = 0, \tag{4.26}$$
$$t_2^* = \frac{(T_l - T_f)}{g},$$
$$t_3 = t_2 - t_2^*,$$

where, l is the thickness of the plate, T_1, T_2, T_3 are the temperatures, a_1, a_2, a_3 are the thermal diffusivities, K_1, K_2, K_3 are thermal conductivities, $\tau_{q_1}, \tau_{q_2}, \tau_{q_3}$ are relaxation time in solid, mushy and liquid region respectively. L is the latent heat, s_1, s_2 are moving fronts present at solid-mush and mush-liquid boundaries respectively. The time t_1, t_2 and t_3 are taken for completion of the stages.

4.2.1 Dimensionless Analysis

Introducing the dimensionless variable

$$x = \frac{r}{l},\ Fo_1 = \frac{a_3 t_1}{l^2},\ Fo_2 = \frac{a_2 t_2}{l^2},\ Fo_3 = \frac{a_1 t_3}{l^2},\ K_{21} = \frac{K_2}{K_1},\ K_{32} = \frac{K_3}{K_2},$$
$$Ste = \frac{C_1(T_l - T_f)}{L},\ Ste_1 = \frac{C_2(T_i - T_l)}{L},\ \lambda_j(Fo_i) = \frac{s_j(t_i)}{l}, j = 1, 2,\ i = 2, 3$$
$$Pd_1 = \frac{gl^2}{a_3(T_i - T_l)},\ Pd_2 = \frac{gl^2}{a_2(T_i - T_l)},\ Pd_3 = \frac{gl^2}{a_1(T_l - T_f)},$$
$$\eta_1 = \frac{a_1\tau_{q_1}}{l^2},\ \eta_2 = \frac{a_2\tau_{q_2}}{l^2},\ \eta_3 = \frac{a_3\tau_{q_3}}{l^2},\ Q_1 = \frac{f_{su_1}}{2Ste_1},\ Q_2 = \frac{f_{su} - f_{su_1}}{2Ste};$$

Stage I

$$\theta_3(x, Fo_1) = \frac{T_i - T_3}{T_i - T_l},$$

Stage II

$$\theta_2(x, Fo_2) = \frac{T_l - T_2}{T_i - T_l},\ \ \theta_3(x, Fo_2) = \frac{T_l - T_3}{T_i - T_l},$$

Stage III

$$\theta_1(x, Fo_3) = \frac{T_1 - T_f}{T_l - T_f},\ \ \theta_2(x, Fo_3) = \frac{T_2 - T_f}{T_l - T_f},\ \theta_3(x, Fo_3) = \frac{T_3 - T_f}{T_l - T_f},$$

and similarity criteria

$$\lambda_1(Fo_i) = 2\lambda_{01}\sqrt{Fo_i},\ \ \lambda_2(Fo_i) = 2\lambda_{02}\sqrt{Fo_i},\ i = 2, 3,$$

where, λ_1, λ_2 are the dimensionless moving fronts present in solid-mush and mush-liquid boundaries respectively. $Fo_i, i = 1, 2, 3$ are Fourier numbers, $\theta_1, \theta_2, \theta_3$ are the dimensionless temperatures. η_1, η_2, η_3 are dimensionless relaxation time in solid, mushy and liquid region. The Eqs. (4.7 - 4.26) reduce in the form of

Stage I

$$\frac{\partial\theta_3}{\partial Fo_1} + \eta_3\frac{\partial^2\theta_3}{\partial Fo_1^2} = \frac{\partial^2\theta_3}{\partial x^2},\ 0 < x < 1. \tag{4.27}$$

The initial and boundary conditions are

$$\theta_3(x, 0) = 0,\ \frac{\partial\theta_3}{\partial Fo_1} = 0, \tag{4.28}$$

$$\theta_3(0, Fo_1) = Pd_1 Fo_1, \tag{4.29}$$

$$\frac{\partial\theta_3(1, Fo_1)}{\partial x} = 0. \tag{4.30}$$

Stage II

In this stage, only mushy-liquid boundary is present put $s_1(t) = 0$ and $T_f = 0$ in Eq. (4.5-4.6) and then substitute it in Eq. (4.10) we get

Case(1): when solid fraction depends on distance

$$\frac{\partial \theta_2}{\partial Fo_2} + \eta_2 \frac{\partial^2 \theta_2}{\partial Fo_2^2} = \frac{\partial^2 \theta_2}{\partial x^2} - \frac{f_{su_1} x}{Ste_1 \lambda_2^2} \frac{d\lambda_2}{dFo_2}, 0 < x < \lambda_2(Fo_2), \tag{4.31}$$

Case(2): when solid fraction depends on temperature

$$\left(1 - \frac{f_{su_1} L}{C_2 T_l}\right) \frac{\partial \theta_2}{\partial Fo_2} + \eta_2 \frac{\partial^2 \theta_2}{\partial Fo_2^2} = \frac{\partial^2 \theta_2}{\partial x^2}, 0 < x < \lambda_2(Fo_2), \tag{4.32}$$

$$\frac{\partial \theta_3}{\partial Fo_2} = a_{32} \frac{\partial^2 \theta_3}{\partial x^2}, \ \lambda_2(Fo_2) < x < 1, \tag{4.33}$$

initial and boundary conditions are

$$\theta_2(x, Fo_1^*) = \theta_3(x, Fo_1^*) = 0, \ \frac{\partial \theta_2(x, Fo_1^*)}{\partial Fo} = 0, \tag{4.34}$$

$$\theta_2(0, Fo_2) = -1 + Pd_2 Fo_2, \tag{4.35}$$

$$\theta_2(\lambda_2(Fo_2), Fo_2) = \theta_3(\lambda_2(Fo_2), Fo_2) = 0, \tag{4.36}$$

$$\frac{\partial \theta_2}{\partial x} - k_{32} \frac{\partial \theta_3}{\partial x} = \frac{f_{su_1}}{Ste_1} \frac{\partial x}{\partial Fo_2}, \ x = \lambda_2(Fo_2) \tag{4.37}$$

$$\frac{\partial \theta_3(1, Fo_2)}{\partial x} = 0, \tag{4.38}$$

$$Fo_1^* = \frac{1}{Pd_1}, Fo_2 = Fo_1 - Fo_1^*.$$

Stage III

$$\frac{\partial \theta_1}{\partial Fo_3} + \eta_1 \frac{\partial^2 \theta_1}{\partial Fo_3^2} = \frac{\partial^2 \theta_1}{\partial x^2}, 0 < x < \lambda_1(Fo_3), \tag{4.39}$$

Using Eq. (4.4 - 4.6) in Eq. (4.18) we get

case(1): when solid fraction depends on distance

$$\frac{\partial \theta_2}{\partial Fo_3} = a_{21} \frac{\partial^2 \theta_2}{\partial x^2} + Q_2 \left(\frac{(\lambda_2 - x)\frac{d\lambda_1}{dFo_3} - (\lambda_1 - x)\frac{d\lambda_2}{dFo_3}}{(\lambda_2 - \lambda_1)^2} \right), \lambda_1(Fo_3) < x < \lambda_2(Fo_3), \tag{4.40}$$

Case(2): when solid fraction depends on temperature

$$\left(1 + \frac{f_{su} - f_{su_1}}{Ste}\right) \frac{\partial \theta_2}{\partial Fo_3} = a_{21} \frac{\partial^2 \theta_2}{\partial x^2}, \lambda_1(Fo_3) < x < \lambda_2(Fo_3), \tag{4.41}$$

$$\frac{\partial \theta_3}{\partial Fo_3} = a_{31} \frac{\partial^2 \theta_3}{\partial x^2}, \lambda_2(Fo_3) < x < 1, \tag{4.42}$$

initial and boundary conditions are

$$\theta_1(x, Fo_2^*) = \theta_2(x, Fo_2^*) = \theta_3(x, Fo_2^*), \frac{\partial \theta_1(x, Fo_2^*)}{\partial Fo_3} = 0, \tag{4.43}$$

$$\theta_1(0, Fo_3) = -Pd_3 Fo_3, \tag{4.44}$$

$$\theta_1(\lambda_1(Fo_3), Fo_3) = \theta_2(\lambda_1(Fo_3), Fo_3) = 0, \tag{4.45}$$

$$\frac{\partial \theta_1}{\partial x} - k_{21}\frac{\partial \theta_2}{\partial x} = \frac{(1 - f_{su})}{Ste}\frac{\partial x}{\partial Fo_3},\ x = \lambda_1(Fo_3), \tag{4.46}$$

$$\theta_2(\lambda_2(Fo_3), Fo_3) = \theta_3(\lambda_2(Fo_3), Fo_3) = 1, \tag{4.47}$$

$$\frac{\partial \theta_2}{\partial x} - k_{32}\frac{\partial \theta_3}{\partial x} = \frac{f_{su_1}}{Ste_1}\frac{\partial x}{\partial Fo_2},\ x = \lambda_2(Fo_3), \tag{4.48}$$

$$\frac{\partial \theta_3(1, Fo_3)}{\partial x} = 0, \tag{4.49}$$

$$Fo_2^* = \frac{1}{Pd_3},\ Fo_3 = Fo_2 - Fo_2^*.$$

4.2.2 Well-Posedness of Model

In order to prove the well-posedness of model we have proved the following two theorems:

Theorem 1 Let $\mathcal{L}$ be an operator on the Hilbert space $L^2[0,1]$ and $\theta, \frac{\partial \theta}{\partial x} \epsilon\ \mathcal{C}^0[0,1]$. If $\theta(0, Fo)$ and $\frac{\partial \theta(0,Fo)}{\partial x}$ are negative for all Fo. Then operator $\mathcal{L}$ is semi bounded.

Proof Let us consider the differential equation

$$b_1\frac{\partial \theta}{\partial Fo} + b_2\frac{\partial^2 \theta}{\partial Fo^2} + f(x) = \mathcal{L}\theta, \tag{4.50}$$

with initial condition

$$\theta(x, Fo^*) = \theta_0, \frac{\partial \theta(x, Fo^*)}{\partial Fo} = g_1(x), \tag{4.51}$$

associated boundary conditions

$$\theta(a(Fo), Fo) = \tau_1(Fo), \frac{\partial \theta(1, Fo^*)}{\partial Fo} = 0,\ 0 \leq a(Fo) \leq 1. \tag{4.52}$$

Now claim $\mathcal{L}$ is semi bounded operator.

$$\langle \theta, \mathcal{L}\theta \rangle_{L^2[0,1]} = -\theta(0, Fo)\frac{\partial \theta(0, Fo)}{\partial x} - \left\langle \frac{\partial \theta}{\partial x}, \frac{\partial \theta}{\partial x} \right\rangle_{L^2[0,1]}$$

$$\langle \theta, (\mathcal{L} + \mathcal{L}^*)\theta \rangle_{L^2[0,1]} = -2\theta(0, Fo)\frac{\partial \theta(0, Fo)}{\partial x} - 2\left\langle \frac{\partial \theta}{\partial x}, \frac{\partial \theta}{\partial x} \right\rangle_{L^2[0,1]}$$

where $\mathcal{L}^*$ is the adjoint operator of $\mathcal{L}$.

$$\langle \theta, (\mathcal{L} + \mathcal{L}^*)\theta \rangle_{L^2[0,1]} \leq 0. \tag{4.53}$$

Hence, $\mathcal{L}$ is semi bounded operator.

Theorem 2 The problem defined in Eq. (4.50 - 4.52) is well-posed if it is semi bounded.

Proof

$$\begin{aligned}
\left(b_1 \frac{d}{dFo} + b_2 \frac{d^2}{dFo^2}\right) \langle \theta, \theta \rangle \quad &= \langle \mathcal{L}\theta - f(x), \theta \rangle + \langle \theta, \mathcal{L}\theta - f(x) \rangle \,, \\
&= \langle \mathcal{L}\theta, \theta \rangle - \langle f(x), \theta \rangle + \langle \theta, \mathcal{L}\theta \rangle - \langle \theta, f(x) \rangle \,, \\
&= \langle \theta, \mathcal{L}^*\theta \rangle + \langle \theta, \mathcal{L}\theta \rangle - 2 \mid \langle \theta, f(x) \rangle \mid, \\
&= \langle \theta, (\mathcal{L} + \mathcal{L}^*)\theta \rangle - 2 \mid \langle \theta, f(x) \rangle \mid .
\end{aligned}$$

By theorem 1, we have proved that $\langle \theta, (\mathcal{L} + \mathcal{L}^*)\theta \rangle \leq 0$. Hence,

$$\left(b_1 \frac{d}{dFo} + b_2 \frac{d^2}{dFo^2}\right) \langle \theta, \theta \rangle \leq -2 \mid \langle \theta, f(x) \rangle \mid, \tag{4.54}$$

using the Cauchy Schwarz inequality we get

$$\left(b_1 \frac{d}{dFo} + b_2 \frac{d^2}{dFo^2}\right) \langle \theta, \theta \rangle \leq -2 \mid\mid\mid \theta \mid\mid_2 \mid\mid f(x) \mid\mid_2 . \tag{4.55}$$

Therefore, We get the solution

$$\mid\mid \theta \mid\mid_2 \leq \left(\frac{g_1(x) - \alpha_2\theta_0}{\alpha_1 - \alpha_2}\right) e^{\alpha_1(Fo - Fo^*)} + \left(\frac{\alpha_1\theta_0 - g_1(x)}{\alpha_1 - \alpha_2}\right) e^{\alpha_2(Fo - Fo^*)}, \tag{4.56}$$

where

$$\alpha_1 = \frac{-b_1 + \sqrt{b_1^2 - 8b_2 \mid f(x) \mid}}{2b_2}, \; \alpha_2 = \frac{-b_1 - \sqrt{b_1^2 - 8b_2 \mid f(x) \mid}}{2b_2}.$$

4.3 Solution of the Problem

To obtain the solution of partial differential Eq. (4.27) associated with initial and boundary conditions defined in Eqs. (4.28 - 4.30), we used the Laplace transform technique and take the inversion of Laplace transform by using Cauchy residual

theorem.

Stage I

$$\theta_3(x, Fo_1) = Pd_1 Fo_1 - Pd_1 x + \frac{Pd_1 x^2}{2} + 4\pi e^{\alpha Fo1} \sum_{\gamma=0}^{\infty} (-1)^{\gamma} \left(\gamma + \frac{1}{2}\right) \times \cos(\gamma + 1/2)(x-1) \left(\frac{A_1 \cos \beta Fo_1 - B_1 \sin \beta Fo_1}{(A_1^2 + B_1^2)}\right), \eta_3 \neq 0. \quad (4.57)$$

where

$$\alpha = \frac{-1}{2\eta_3}, \quad \beta = \frac{\sqrt{4(\gamma + 1/2)^2 \pi^2 \eta_3 - 1}}{2\eta_3},$$
$$A_1 = (\alpha^2 - \beta^2)(1 + 2\eta_3 \alpha) - 4\eta_3 \alpha \beta^2, \quad B_1 = 2\eta_3 \beta(\alpha^2 - \beta^2) + 2\alpha\beta(1 + 2\eta_3 \alpha).$$

For Fourier model $\eta_3 = 0$, the inversion of Laplace transform is

$$\theta_3(x, Fo_1) = Pd_1(x^2/2 - x + Fo_1) + 2Pd_1 Fo_1 \sum_{\gamma=0}^{\infty} \left(\frac{e^{(\gamma+\frac{1}{2})^2 \pi^2} \sin(\gamma + \frac{1}{2})\pi x}{(\gamma + \frac{1}{2})^3 \pi^3}\right). \quad (4.58)$$

4.3.1 Legendre Wavelets Spectral Galerkin Method

To solve the stage II and stage III, we are developing the Legendre wavelets spectral Galerkin method because the interface boundary is moving with the time and to obtain the exact solution in these stages is difficult task. In this method we assumed the solution in the form of second derivative is a linear combination of Legendre wavelets basis function i.e.

$$\frac{\partial^2 \theta_i}{\partial x^2} \simeq C_i^T(Fo_i)\psi(x), i = 1, 2, 3, \quad (4.59)$$

where $C_i(Fo_i)$ and $\psi(x)$ are the column vector of order $2^{k-1}M \times 1$ which are defined as:

$$C_i(Fo_i) = [c_{10}^i(Fo_i), c_{11}^i(Fo_i), c_{12}^i(Fo_i) \cdots, c_{1M-1}^i(Fo_i), c_{20}^i(Fo_i), \cdots, c_{2M-1}^i(Fo_i), \cdots, c_{2^{k-1}0}^i(Fo_i) \cdots, c_{2^{k-1}M-1}^i(Fo_i)]^T, i = 1, 2, 3, \quad (4.60)$$

and

$$\psi(x) = [\psi_{10}(x), \psi_{11}(x), \cdots \psi_{1M-1}(x), \psi_{20}(x), \cdots, \psi_{2M-1}(x), \cdots \psi_{2^{k-1}0}(x), \cdots \psi_{2^{k-1}M-1}(x)]^T \quad (4.61)$$

respectively. The elements of column vector ψ are known as Legendre wavelets which is defined in Eq. (1.87). Integrating Eq. (4.59) two times from 0 to x and using property of operational matrix of integration defined in Eq. (1.92), we get

$$\frac{\partial \theta_i}{\partial x}(x, Fo_i) = \frac{\partial \theta_i}{\partial x}(0, Fo_i) + C_i^T(Fo_i)P\psi(x), \tag{4.62}$$

$$\theta_i(x, Fo_i) = \theta_i(0, Fo_i) + \frac{\partial \theta_i}{\partial x}(0, Fo_i)d^T P\psi(x) + C_i^T(Fo_i)P^2\psi(x). \tag{4.63}$$

Using the associated boundary conditions for elimination of $\theta_i(0, Fo_i)$ and $\frac{\partial \theta_i}{\partial x}(0, Fo_i)$ from Eqs. (4.35 - 4.37), Eq. (4.39), Eqs. (4.44 - 4.46) and Eq. (4.48), Eq. (4.50). After this we substitute θ_i, $\frac{\partial \theta_i}{\partial x}$ and $\frac{\partial^2 \theta_i}{\partial x^2}$ in the differential equation came from stage II - III, we get the residuals $R_i\left(C_i, \frac{dC_i}{dFo_i}, \frac{d^2C_i}{dFo_i{}^2}, x, Fo_i\right)$. Using Galerkin approach in such a way that the residuals obtained from differential equations are orthogonal to Legendre wavelets basis function i.e.,

$$\int_0^1 R_i\left(C_i, \frac{dC_i}{dFo_i}, \frac{d^2C_i}{dFo_i{}^2}, x, Fo_i\right)\psi(x)dx = 0. \tag{4.64}$$

After simplification of Eq. (4.64), we get the system of initial value problem given by

$$X_i\frac{d^2C_i}{dFo_i{}^2} + Y_i\frac{dC_i}{dFo_i} + Z_iC_i = G_i, \tag{4.65}$$

$$\frac{dC_i}{dFo_i}(Fo_j^*) = H_{1i},\ C_i(Fo_j^*) = H_{0i}, i = 1, 2, 3, j = 1, 2, \tag{4.66}$$

of order $2^{k-1}M \times 1$. for stage II and stage III, the coefficients X_i, Y_i, Z_i of order $2^{k-1}M \times 2^{k-1}M$ are given below

Stage II when solid fraction is distance dependent

$$X_2 = \eta_2\left(P^{2T} - P^T d\left(\frac{\psi(\lambda_2)}{\lambda_2}\right)^T P^{2T}\right),$$

$$Y_2 = P^{2T} - P^T d\left(\frac{\psi(\lambda_2)}{\lambda_2}\right)^T P^{2T} - 2\eta_2 P^T d\left(\frac{\psi(\lambda_2)}{\lambda_2}\right)^{'T} P^{2T},$$

$$Z_2 = -P^T d\left(\frac{\psi(\lambda_2)}{\lambda_2}\right)^{'T} P^{2T} - \eta_2 P^T d\left(\frac{\psi(\lambda_2)}{\lambda_2}\right)^{''T} P^{2T} - I,$$

$$G_2 = -Pd_2 d - P^T d\left(\frac{1 - Pd_2Fo_2}{\lambda_2}\right)^{'T} - \eta_2 P^T d\left(\frac{1 - Pd_2Fo_2}{\lambda_2}\right)^{''T} P^{2T} - \frac{f_{su_1}P^T d}{2Ste_1\lambda_2 Fo_2}.$$

When Solid fraction is temperature dependent.

$$Y_2 = P^{2T} - \zeta P^T d \left(\frac{\psi(\lambda_2)}{\lambda_2}\right)^T P^{2T} - 2\eta_2 P^T d \left(\frac{\psi(\lambda_2)}{\lambda_2}\right)^{'T} P^{2T},$$

$$Z_2 = -\zeta P^T d \left(\frac{\psi(\lambda_2)}{\lambda_2}\right)^{'T} P^{2T} - \eta_2 P^T d \left(\frac{\psi(\lambda_2)}{\lambda_2}\right)^{''T} P^{2T} - I,$$

$$G_2 = -\zeta P d_2 d - \zeta P^T d \left(\frac{1 - P d_2 F o_2}{\lambda_2}\right)^{'T} - \eta_2 P^T d \left(\frac{1 - P d_2 F o_2}{\lambda_2}\right)^{''T} P^{2T} - \frac{f_{su_1} P^T d}{2 S t e_1 \lambda_2 F o_2}.$$

Where, $\zeta = (1 - \frac{f_{su_1} L}{C_2 T_l})$.

$$H_{02} = \frac{\lambda_2(1 - P d_2 F o_1^*)d - P^T d(1 - P d_2 F o_1^*) + \lambda_2 \int_0^1 \theta_3(x, F o_1^*) dx}{\lambda_2 P^{2T} - P^T d \psi^T(\lambda_2) P^{2T}},$$

$$H_{12} = \frac{P^T d(\frac{\psi(\lambda_2)}{\lambda_2})' P^{2T} H_{02} - P^T d(\frac{(1 - P d_2 F o_1^*)}{\lambda_2})' - P d_2 d}{P^{2T} - P^T d \frac{\psi(\lambda_2)}{\lambda_2} P^{2T}},$$

In liquid region;

$$Y_3 = \lambda_2 d\psi^T(1) P^T - d\psi^T(\lambda_2) P^{2T} - P^T d\psi^T(1) P^T + P^{2T},$$

$$Z_3 = \lambda_2^{'} d\psi^T(1) P^T - d\psi^{'T}(\lambda_2) P^{2T} - a_{32} I,$$

$$H_{03} = \frac{\int_0^1 \theta_3(x, F o_1^*) dx}{(\lambda_2 d\psi^T(1) P^T - d\psi^T(\lambda_2) P^{2T} - P^T d\psi^T(1) P^T + P^{2T})}.$$

Stage III In solid region,

$$X_1 = \eta_1 \left(P^{2T} - P^T d \left(\frac{\psi(\lambda_1)}{\lambda_1}\right)^T P^{2T}\right),$$

$$Y_1 = P^{2T} - P^T d \left(\frac{\psi(\lambda_1)}{\lambda_1}\right)^T P^{2T} - 2\eta_1 P^T d \left(\frac{\psi(\lambda_1)}{\lambda_1}\right)^{'T} P^{2T},$$

$$Z_1 = -P^T d \left(\frac{\psi(\lambda_1)}{\lambda_1}\right)^{'T} P^{2T} - \eta_1 P^T d \left(\frac{\psi(\lambda_1)}{\lambda_1}\right)^{''T} P^{2T} - I,$$

$$G_1 = -P d_3 d + P d_3 P^T d \left(\frac{F o_3}{\lambda_2}\right)^{'T} + \eta_1 P d_3 P^T d \left(\frac{F o_3}{\lambda_2}\right)^{''T} P^{2T},$$

$$H_{01} = \frac{\lambda_1 P d_3 F o_2^* - P d_3 F o_2^* P^T d + \int_0^1 \theta_2(x, F o_2^*) dx}{\lambda_1 P^{2T} - P^T d \psi(\lambda_1) P^{2T}},$$

$$H_{11} = \frac{P d_3 F o_2^* - (\frac{P d_3 F o_2^*}{\lambda_1})' P^T d + P^T d(\frac{\psi(\lambda_1)}{\lambda_1})' P^{2T} H_{01}}{P^{2T} - P^T d(\frac{\psi(\lambda_1)}{\lambda_1})^T P^{2T}}.$$

In mushy region, when solid fraction depends on distance

$$
\begin{aligned}
Y_2 = \quad & \frac{\lambda_1}{\lambda_1-\lambda_2} d\psi^T(\lambda_1)P^{2T} - \frac{\lambda_1}{\lambda_1-\lambda_2} d\psi^T(\lambda_2)P^{2T} + P^T d\left(\frac{\psi(\lambda_2)}{\lambda_1-\lambda_2}\right)^T P^{2T} \\
& -P^T d\left(\frac{\psi(\lambda_1)}{\lambda_1-\lambda_2}\right)^T P^{2T} + P^{2T} - d\psi^T(\lambda_1)P^{2T}, \\
Z_2 = \quad & \frac{\lambda_1}{\lambda_1-\lambda_2} d\psi'^T(\lambda_1)P^{2T} - \frac{\lambda_1}{\lambda_1-\lambda_2} d\psi'^T(\lambda_2)P^{2T} + P^T d\left(\frac{\psi(\lambda_2)}{\lambda_1-\lambda_2}\right)'^T P^{2T} \\
& -P^T d\left(\frac{\psi(\lambda_1)}{\lambda_1-\lambda_2}\right)'^T P^{2T} - d\psi'^T(\lambda_1)P^{2T} - a_{21}I, \\
G_2 = \quad & -\left(\frac{1}{\lambda_1-\lambda_2}\right)' P^T d + \frac{Q_2 P^T d}{(\lambda_1-\lambda_2)Fo_3}.
\end{aligned}
$$

In mushy region, when solid fraction depends on temperature

$$
\begin{aligned}
Y_2 = \quad & (1+Q_2)\left(\frac{\lambda_1}{\lambda_1-\lambda_2} d\psi^T(\lambda_1)P^{2T} - \frac{\lambda_1}{\lambda_1-\lambda_2} d\psi^T(\lambda_2)P^{2T} + P^T d\left(\frac{\psi(\lambda_2)}{\lambda_1-\lambda_2}\right)^T P^{2T}\right) \\
& +(1+Q_2)\left(-P^T d\left(\frac{\psi(\lambda_1)}{\lambda_1-\lambda_2}\right)^T P^{2T} + P^{2T} - d\psi^T(\lambda_1)P^{2T}\right), \\
Z_2 = \quad & (1+Q_2)\left(\frac{\lambda_1}{\lambda_1-\lambda_2} d\psi'^T(\lambda_1)P^{2T} - \frac{\lambda_1}{\lambda_1-\lambda_2} d\psi'^T(\lambda_2)P^{2T} + P^T d\left(\frac{\psi(\lambda_2)}{\lambda_1-\lambda_2}\right)'^T P^{2T}\right) \\
& +(1+Q_2)\left(-P^T d\left(\frac{\psi(\lambda_1)}{\lambda_1-\lambda_2}\right)'^T P^{2T} - d\psi'^T(\lambda_1)P^{2T}\right) - a_{21}I, \\
G_2 = \quad & (1+Q_2)\left(\frac{1}{\lambda_1-\lambda_2}\right)' P^T d,
\end{aligned}
$$

$$
H_{02} = \frac{\frac{P^T d}{\lambda_1-\lambda_2} - \frac{\lambda_1 d}{\lambda_1-\lambda_2} + \int_0^1 \theta_2(x, Fo_2^*)dx}{\frac{\lambda_1}{\lambda_1-\lambda_2}(d\psi^T(\lambda_1)P^{2T} - d\psi^T(\lambda_2)P^{2T}) - d\psi^T(\lambda_1)P^{2T} - P^T d(\frac{\psi(\lambda_1)}{\lambda_1-\lambda_2})^T P^{2T} + P^T d(\frac{\psi(\lambda_2)}{\lambda_1-\lambda_2})^T P^{2T} + P^{2T}}.
$$

In liquid region

$$
\begin{aligned}
Y_3 = \quad & \lambda_2 d\psi^T(1)P^T - d\psi^T(\lambda_2)P^{2T} - P^T d\psi^T(1)P^T + P^{2T}, \\
Z_3 = \quad & \lambda_2' d\psi^T(1)P^T - d\psi'^T(\lambda_2)P^{2T} - a_{31}I, \\
H_{03} = \quad & \frac{-d + \int_0^1 \theta_2(x, Fo_2^*)dx}{(\lambda_2 d\psi^T(1)P^T - d\psi^T(\lambda_2)P^{2T} - P^T d\psi^T(1)P^T + P^{2T})}.
\end{aligned}
$$

For solution of the system of initial value problem Eq.(4.65 - 4.66), using Taylor series expansion method as follows

$$
C_i(Fo_i) = \sum_{\gamma=0}^{\infty} \frac{\left(Fo_i - Fo_j^*\right)^\gamma}{\gamma!} \frac{d^\gamma C_i}{dFo_i{}^\gamma}(Fo_j^*),\ i = 1,2,3,\ \ j = 1,2. \tag{4.67}
$$

Substituting $C_i(Fo_i)$ in Eq. (4.63), we get the temperature $\theta_i(x, Fo_i),\ i = 1, 2, 3$ in each stages as

$$\theta_i(x, Fo_i) = \theta_i(0, Fo_i) + \frac{\partial \theta_i}{\partial x}(0, Fo_i) d^T P \psi(x) + \left(\sum_{\gamma=0}^{\infty} \frac{\left(Fo_i - Fo_j^* \right)^{\gamma}}{\gamma!} \frac{d^{\gamma} C_i}{dFo_i{}^{\gamma}} (Fo_j^*) \right)^T P^2 \psi(x). \tag{4.68}$$

4.3.2 Moving Layer Thickness

In stage 2, Eq. (4.38) represents the interface condition for mushy-liquid region and in stage 3, Eq. (4.47), Eq. (4.49) represent the interface condition for solid-mushy and mushy-liquid region respectively. For determining the moving layer thickness, substitute Eq. (4.68) in Eq. (4.38), we get the non linear equation in λ_{02}, and Fo_2. To solve this equation we used Newton-Raphson method for specific time and obtained the value of λ_{02}. Similarly, substitute Eq. (4.68) in Eq. (4.47) and Eq. (4.49) we obtained system of two nonlinear equations in $\lambda_{01}, \lambda_{02}, Fo_3$. To solve these system simultaneously by Newton-Raphson method for specific time and obtained the value of λ_{01} and λ_{02}.

4.3.3 Stability Analysis

Theorem 3 The scheme of Legendre wavelets spectral Galerkin method defined in subsection 4.4.1 is stable.

proof Let $\mathcal{L}\theta_N = C^T(Fo)\psi(x)$. The operator $\mathcal{L}\theta_N$ is semi bounded operator for weight function $w(x) = \psi(x)$

$$\left\langle b_1 \frac{\partial \theta_N}{\partial t} + b_2 \frac{\partial^2 \theta_N}{\partial t^2} - f(x), \theta_N \right\rangle_w = \langle \mathcal{L}\theta_N, \theta_N \rangle_w ,$$

the left hand side of equation is

$$b_1 \frac{1}{2} \frac{d}{dt} \langle \theta_N, \theta_N \rangle + \frac{1}{2} b_2 \frac{d^2}{dt^2} \langle \theta_N, \theta_N \rangle - \langle f(x), \theta_N \rangle ,$$

Right hand side

$$\langle \mathcal{L}\theta_N, \theta_N \rangle_w = \int_0^1 \theta_N \frac{\partial^2 \theta_N}{\partial x^2} dx \leq 0,$$

Therefore, $b_1 \frac{d}{dt} \langle \theta_N, \theta_N \rangle + b_2 \frac{d^2}{dt^2} \langle \theta_N, \theta_N \rangle \leq 0$ (from Eq. (4.57)). Hence, the Legendre wavelets spectral Galerkin method is stable.

4.4 Numerical Computation and Discussion

We developed the time relaxation model for solidification of binary alloy. The process of solidification is completed into three stages defined in Eqs. (4.7 - 4.26). For simplicity of the model we introduced the dimensionless parameters defined in sub-section 4.2.1. Therefore, the dimensionless form of the model is given in Eqs. (4.27 - 4.50). Further, in sub-section 4.2.2 we proved the well-posedness of model. From Theorem 1 and Theorem 2, we observed that our model has a unique solution. For solution of non-dimensional form of the model, we solved the stage I by Laplace transform method, because in stage I, the model is boundary value problem of linear partial differential equation in finite domain. In stage II and Stage III, the model is moving boundary problem of partial differential equations. Therefore, the solution of problem is very difficult task. Because of this we developed the Legendre wavelets spectral Galerkin method given in section 4.3.1. The stability of present method is provided in Theorem 3 given in sub-section 4.3.3. From Theorem 3, we conclude that the Legendre wavelets spectral Galerkin method is unconditionally stable.

For Numerical computation, we have taken $Al - Cu$ binary system containing 5 percent Cu. The properties of $Al - Cu$ alloy (Tien and Geiger (1967)) is given below in Table (4.1).

Table 4.1: Thermo-physical properties of $Al - Cu$ alloy

T_i	648.9 $^\circ C$	T_l	642.2 $^\circ C$
T_f	547.8 $^\circ C$	K_1	197.3 $W/m^\circ C$
K_3	181.73 $W/m^\circ C$	ρ	2723.2 kg/m^3
C_1	1046.7$Ws/Kg^\circ C$	C_3	1256.7 $Ws/Kg^\circ C$
L	395403 Ws/Kg	f_{su}	0.8952

$K_2 = \frac{K_1+K_3}{2} = 185.5 W/m^\circ C, \quad C_2 = \frac{C_1+C_3}{2} = 1151.35\ Ws/Kg^\circ C.$

We have considered solid fraction at liquid-mushy boundary is $f_{su_1} = 0.1041$ and length of plate $l = 0.24m$. For numerical computation we have used Matlab ($R2012a$).

Stage I: In stage I, Fig. (4.1) shows the graph between dimensionless temperature (θ_3) and dimensionless space (x) for different value of dimensionless time Fo_1. In this case we have taken $Pd = 4$ and dimensionless relaxation time $\eta_3 = 0.0277$. As space coordinate

x increases the dimensionless temperature decreases and dimensionless temperature increases when dimensionless time increases. That means the binary alloy $Al-Cu$ is cooled from initial temperature T_i to T_l, the temperature (T_3) decreases as thermal diffusivity of liquid (a_3), time t_3 and space coordinate r is increases.

In stage II and stage III the solid fraction f_s is described in two ways:

- When the solid fraction f_s depends on distance
- When the solid fraction f_s depends on temperature

Case(1): The solid fraction f_s depends on distance

Stage II: For numerical computation we take 5 Legendre wavelets basis functions ($M = 5, k = 1$). When liquid is cooled the mushy region starts to form and takes the time from $1/Pd_1 < Fo_2 < 1/Pd_3$ to complete this stage. In this stage, we take $Pd_1 = 4, Pd_2 = 3.5891, Pd_3 = 0.2177$. The relaxation time in mushy region is taken as $\eta_2 = 0.0462$. The liquidus moving front $\lambda_2 = 0.0890$ is calculated at time $Fo_2 = 0.28$. The dimensionless form of the temperatures, the liquidus moving front and the solid fraction are shown in Figs. (4.2 - 4.5). In Fig. (4.2) the dimensionless temperatures in mushy region and liquid region increases as the dimensionless space coordinate x increases. By the definition of θ_2, θ_3 in sub-section 4.3.1 of stage 2, we conclude that T_2, T_3 decreases as space coordinate r increases. From Fig. (4.3) the dimensionless temperature in mushy region $0 < x < \lambda_2(Fo_2)$ increase for certain time and after that the temperature is decreased as dimensionless time Fo_2 increases at $x = 0.3$. The dimensionless temperature in liquid region decreases as dimensionless time Fo_2 increases at $x = 0.45$. In Fig. (4.4), the dimensionless liquidus front (λ_2) in mushy zone $0 < x < \lambda_2(Fo_2)$ increases as Fo_2 increases. That means, the liquidus moving front (s_2) increases as thermal diffusivity of mushy zone increases and time t_2 increases. From Fig. (4.5), the dimensionless solid fraction present in mushy zone is start to form and increases as the space coordinate x increases.

Stage III: When liquid is continuously cooled the solid is start to form when $Fo_3 > 1/Pd_3$. The value of $Pd_3 = 0.2177, \eta_1 = 0.002$ are taken and the solidus moving front $\lambda_1 = 0.3193$ and liquidus moving front $\lambda_2 = 0.3931$ are calculated at $Fo_3 = 5$. In this stage, we have studied the dimensionless temperatures in solid region, mushy region and liquid region with space coordinate x and time (Fo_3), the solidus and liquidus moving fronts and the solid fraction respectively. It is clear from Fig. (4.6) the temperatures

in solid and mushy region increases as increases the space coordinate x and decreases in liquid region as increases the space coordinate x. In binary system, the temperature of the melt depends upon the specific heat of the individual component. Thus in case, the component has high specific heat is rejected in the melt. the temperature of melt reduces as more heat is required to change the overall temperature of the melt. The temperature of melt reduces as more heat is required to change the overall temperature of the melt. During solidification of $Al - Cu$ alloy such condition may prevail when Al is rejected. In Fig. (4.7), the temperature in mushy and liquid region decreases at $x = 0.65, x = 0.85$ respectively as the time Fo_3 increases while in solid region the temperature is constant at $x = 0.45$. Fig. (4.8) shows the dimensionless solidus ($\lambda_1(Fo_3)$) and liquidus ($\lambda_2(Fo_3)$) moving fronts which separates the solid-mushy region and mushy-liquid region respectively. The solidus moving front ($\lambda_1(Fo_3)$) and liquidus moving front ($\lambda_2(Fo_3)$) increases as the time increases. In this figure, we observed that the liquidus moving front moves fast with respect to solidus moving front. In this case also the solidus moving front $s_1(t_3)$ and liquidus moving front $s_2(t_3)$ increases as thermal diffusivity of solid a_1 increases and time t_3 increases. The solid fraction f_s in mushy zone is shown in Fig. (4.9) and decreases as the space coordinate x increases. In this stage, the solid region starts to form and increases with time therefore, the solid fraction present in mushy region decreases.

Case(2): The solid fraction f_s depends on temperature

Stage II: In this case, the liquidus moving front $\lambda_2 = 0.0489$ is calculated at time $Fo_2 = 0.28$, for the value of $Pd_2 = 3.5891, \eta_2 = 0.0489$. Fig. (4.10) shows the dimensionless temperature in mushy-liquid regions and it increases in both mushy and liquid region as the space coordinate x increases. Fig. (4.11) shows the temperature in mushy-liquid region with time Fo_2 and it is clear from figure that the dimensionless temperature in mushy region increases at $x = 0.3$ with increases the time Fo_2 and in liquid region at $x = 0.45$ it becomes a constant. Fig. (4.12) shows the dimensionless moving layer thickness $\lambda_2(Fo_2)$ in mushy-liquid region and increases as the time $1/Pd_1 < Fo_2 < 1/Pd_3$ increases. Fig. (4.13) shows that the effect of solid fraction f_s on dimensionless space x in mushy region $0 < x < \lambda_2(Fo_2)$. In this region, the solid fraction f_s present in mushy region increases as the dimensionless space x increases.

Stage III: In this stage, the solidus moving front $\lambda_1 = 0.2573$ and the liquidus moving fronts $\lambda_2 = 0.4729$ are calculated at time $Fo_3 = 5$, for $Pd_3 = 0.2177$ and relaxation time $\eta_1 = 0.002$. Figs. (4.14 - 4.17) show the dimensionless form of temperatures in solid,

mushy and liquid region, the dimensionless moving fronts in solid-mushy and mushy-liquid region and the solid fraction present in mushy region respectively. From Fig. (4.14) we conclude that the dimensionless temperature in solid, mushy and liquid region increases as space coordinate x increases. In solidification of $Al - Cu$ alloy, the temperature in liquid region is increased due to rejection of Cu. Fig. (4.15) shows that the dimensionless temperature in liquid, mushy and solid region and decreases as the time Fo_3 increases at $x = 0.85, x = 0.65$ and $x = 0.45$ respectively. Fig. (4.16) shows that the dimensionless moving fronts in solid-mushy and mushy-liquid region and increases as time $Fo_3 > 1/Pd_3$ increases. We observed that the dimensionless moving front in liquidus region moves fast as compare to solidus moving front. Therefore, the temperature in mushy region is taking less time while the solid region takes more time for solidification. In Fig. (4.17), we have shown the effect of solid fraction on dimensionless space x. In this Fig. we observed that as solid fraction f_s decreases in mushy region $\lambda_1(Fo_3) < x < \lambda_2(Fo_3)$ as dimensionless space x increases. In this region, the solid starts to form and the solid fraction presents in mushy region now decreases. Further, the effect of relaxation time on dimensionless temperature in liquid, mushy and solid region are shown in Figs. (4.18 - 4.20) respectively. In Fig. 18 we have compared the Fourier model with non Fourier model. As Predvoditelev number (Pd_1) increases with time Fo_1 for relaxation time $\eta_3 = 0.05$, the non Fourier model coincide with Fourier model. In Fig. (4.19) and Fig. (4.20) we observed that in mushy and solid region, the effect of relaxation time is diminished. That means, the effect of relaxation time is presented only in liquid region and after sometimes the effect will be negligible.

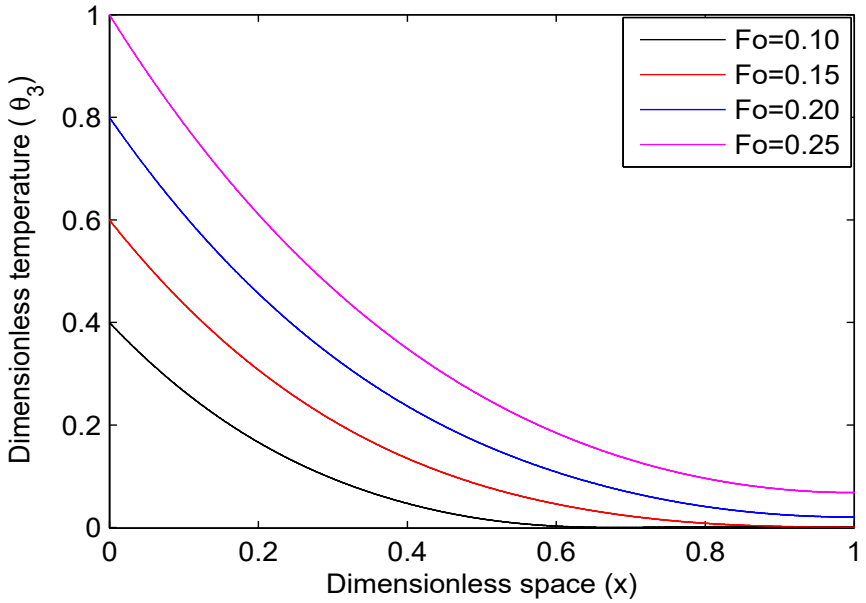

Figure 4.1: Dimensionless temperature with dimensionless space x in stage I, $Pd_1 = 4, \eta_3 = 0.0277$.

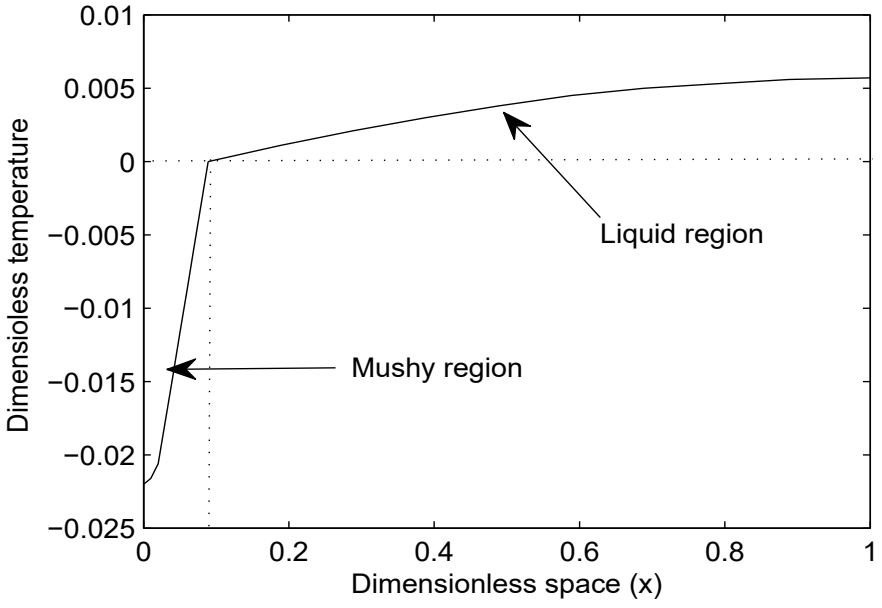

Figure 4.2: Dimensionless temperatures in mushy and liquid regions with dimensionless space x in stage II, $Pd_2 = 3.5891, \eta_2 = 0.0462, \lambda_2 = 0.0890, Fo_3 = 0.28$.

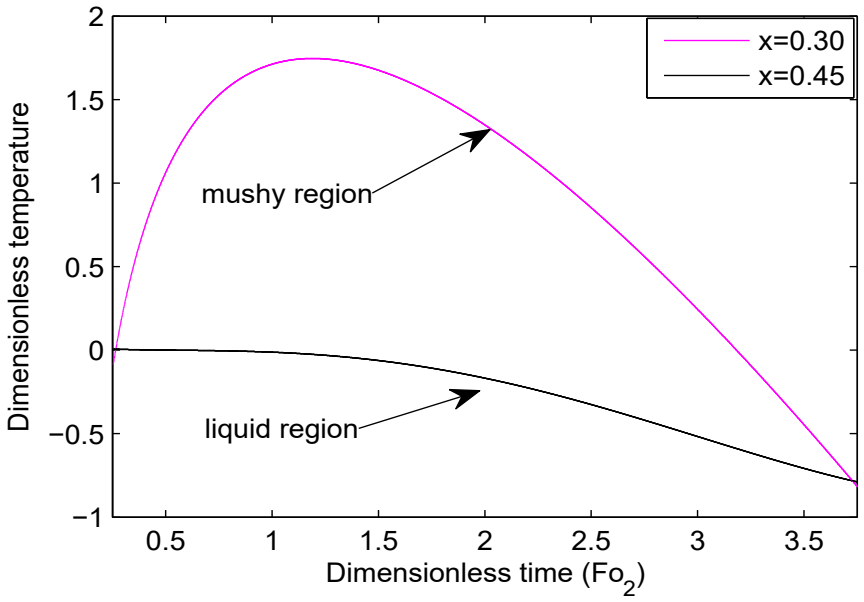

Figure 4.3: Dimensionless temperatures with time Fo_2 in stage 2, $Pd_2 = 3.5891, \eta_2 = 0.0462, \lambda_2 = 0.0890$ (1).

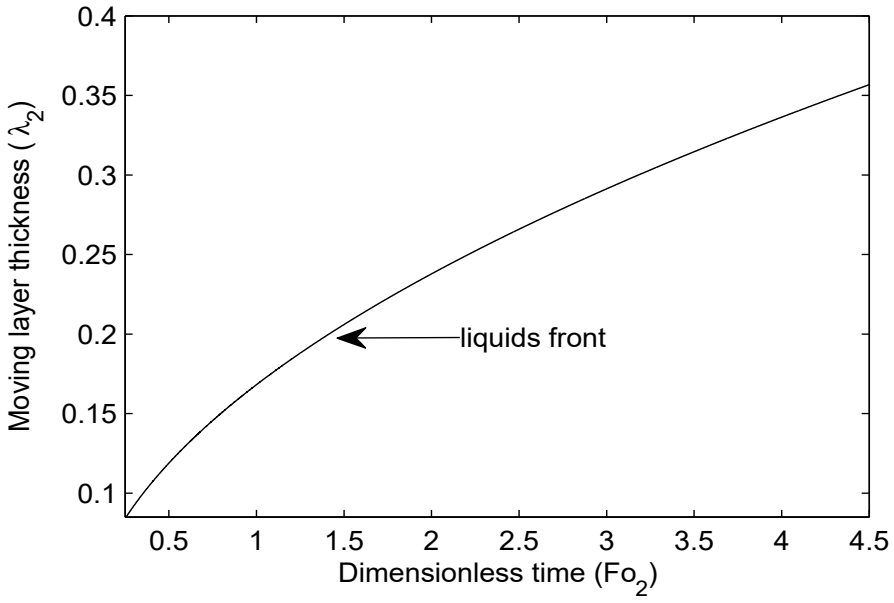

Figure 4.4: Moving layer thickness (λ) with dimensionless time Fo_2.

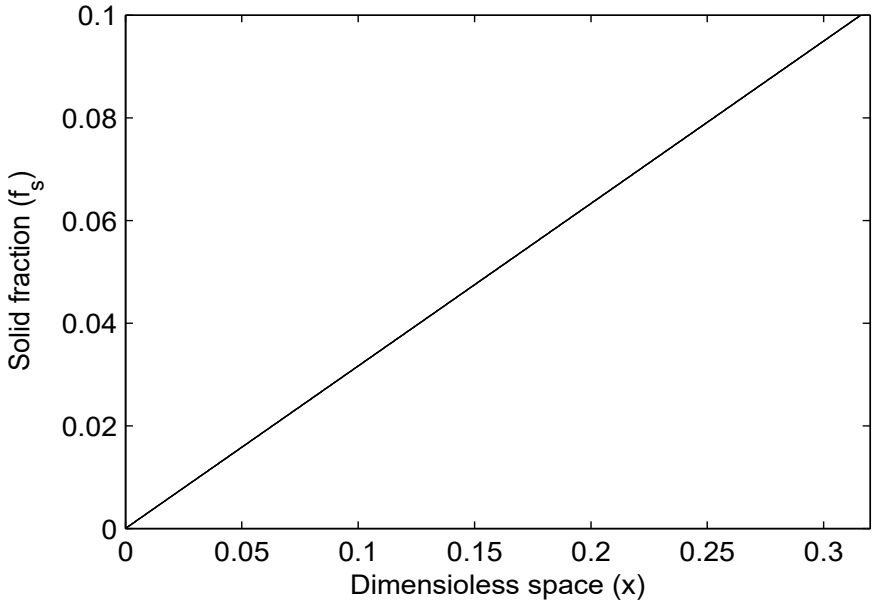

Figure 4.5: Solid fraction (f_s) in mushy zone with dimensionless space x in stage 2, $Fo_2 = 0.25$ (1).

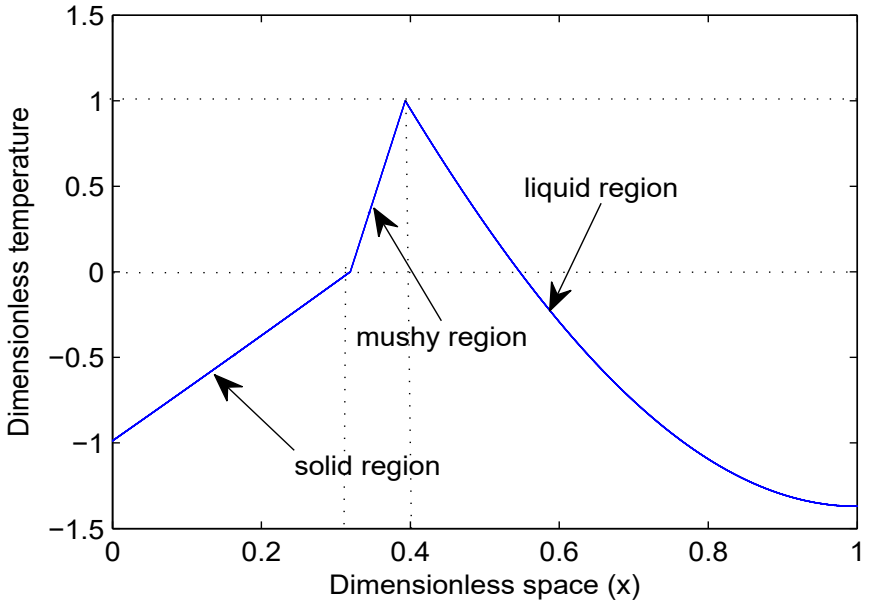

Figure 4.6: Dimensionless temperatures in solid, mushy and liquid region with dimensionless Space x in stage 3 (1), $Pd_3 = 0.2177, \lambda_1 = 0.3193, \lambda_2 = 0.3931, Fo_3 = 5$.

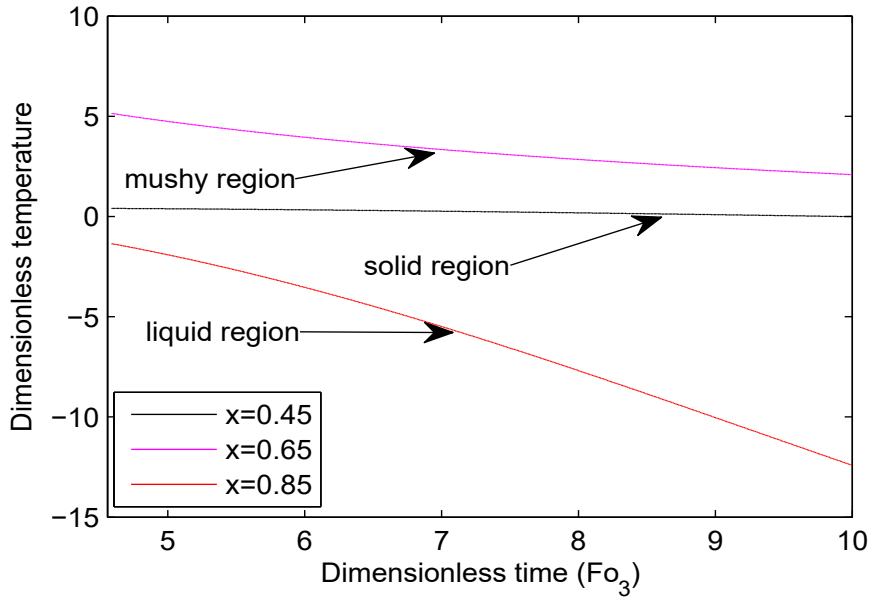

Figure 4.7: Dimensionless temperatures with time Fo_3 in stage 3 (1).

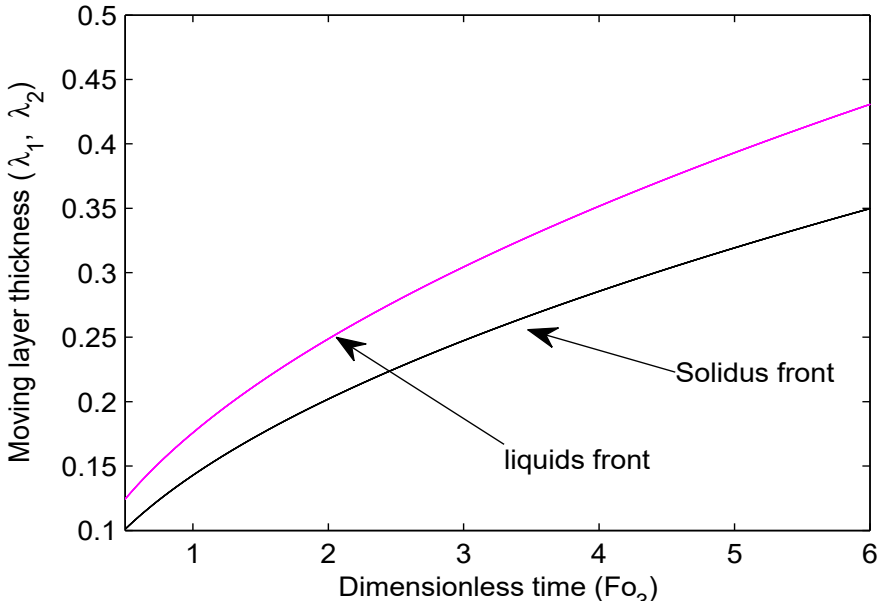

Figure 4.8: Moving layer thickness (λ_1, λ_2) with dimensionless time Fo_3 in stage 3 (1).

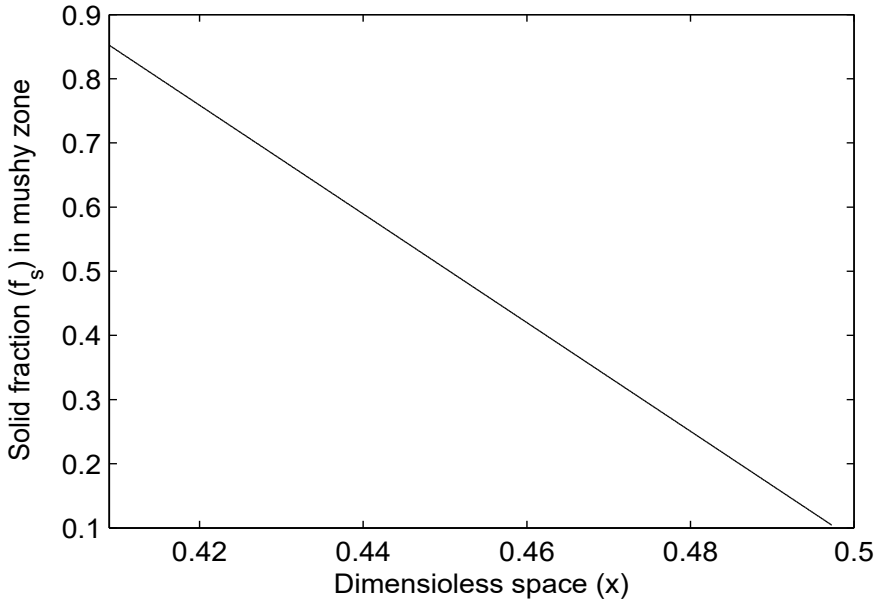

Figure 4.9: Solid fraction (f_s) in mushy region with dimensionless space x in stage 3 (1).

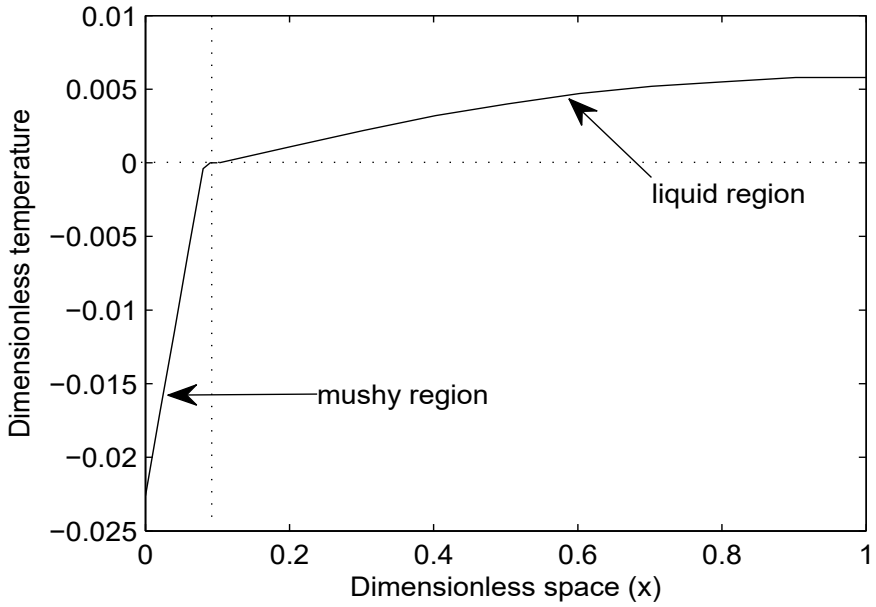

Figure 4.10: Dimensionless temperatures in mushy and liquid regions with dimensionless space x in stage 2 (2), $Pd_2 = 3.5891, \eta_2 = 0.0462, \lambda_2 = 0.0489, Fo_2 = 0.28$.

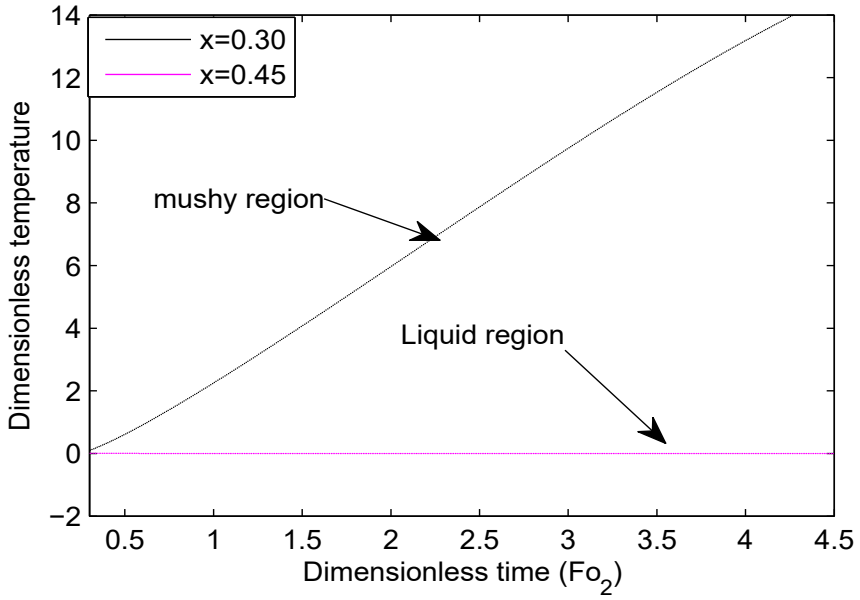

Figure 4.11: Dimensionless temperatures with time Fo_2 in stage 2 (2), $Pd_2 = 3.5891, \eta_2 = 0.0462, \lambda_2 = 0.0489$.

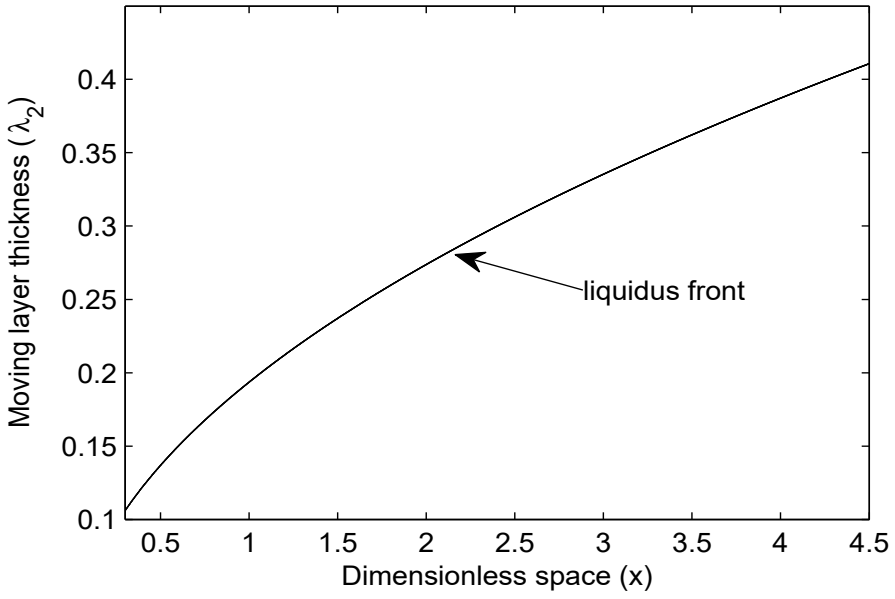

Figure 4.12: Moving layer thickness (λ_2) with dimensionless time Fo_2 in stage 2 (2).

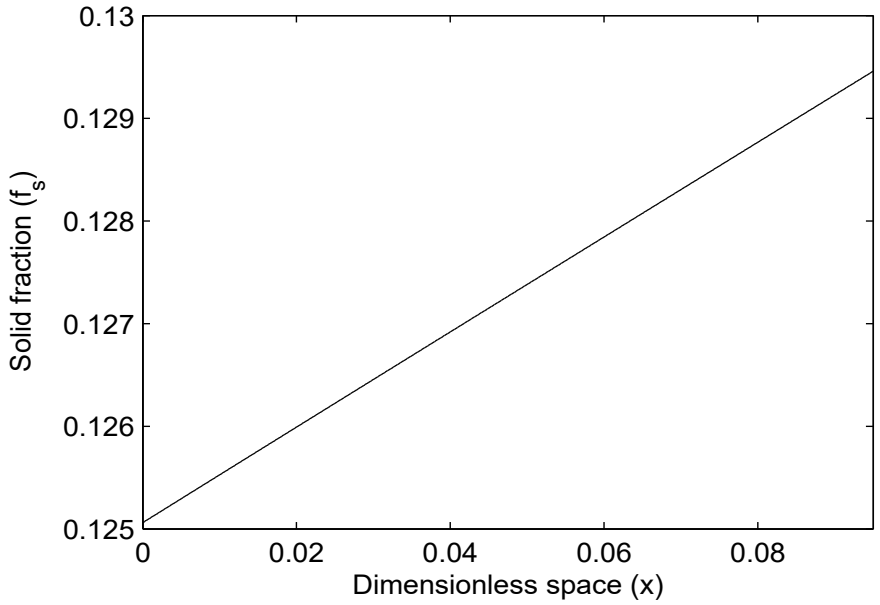

Figure 4.13: Solid fraction (f_s) in mushy region with dimensionless space x in stage 2, $Fo_2 = 0.25$ (2).

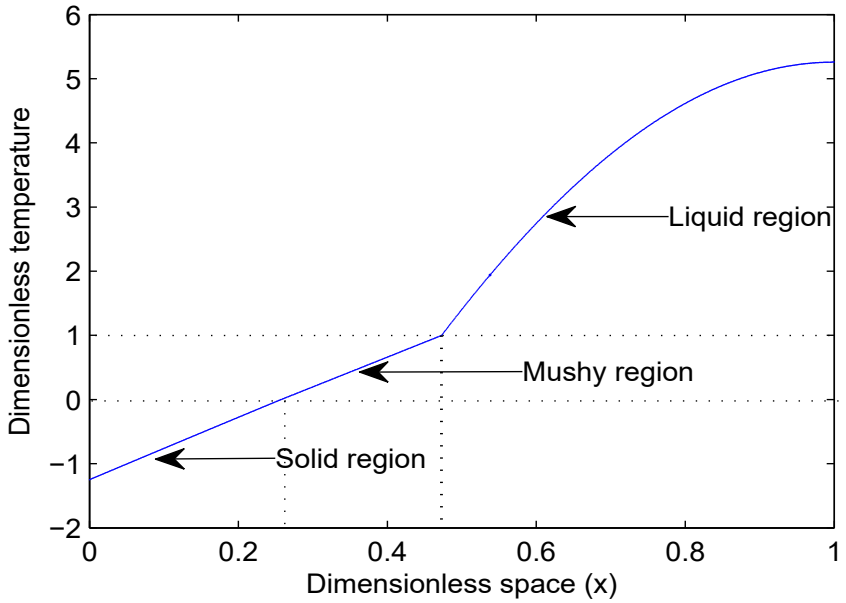

Figure 4.14: Dimensionless temperatures in solid, mushy and liquid regions with dimensionless space x in stage III, $Pd_3 = 0.2177, \eta_1 = 0.002, \lambda_1 = 0.2573, \lambda_2 = 0.4729, Fo_3 = 5$.

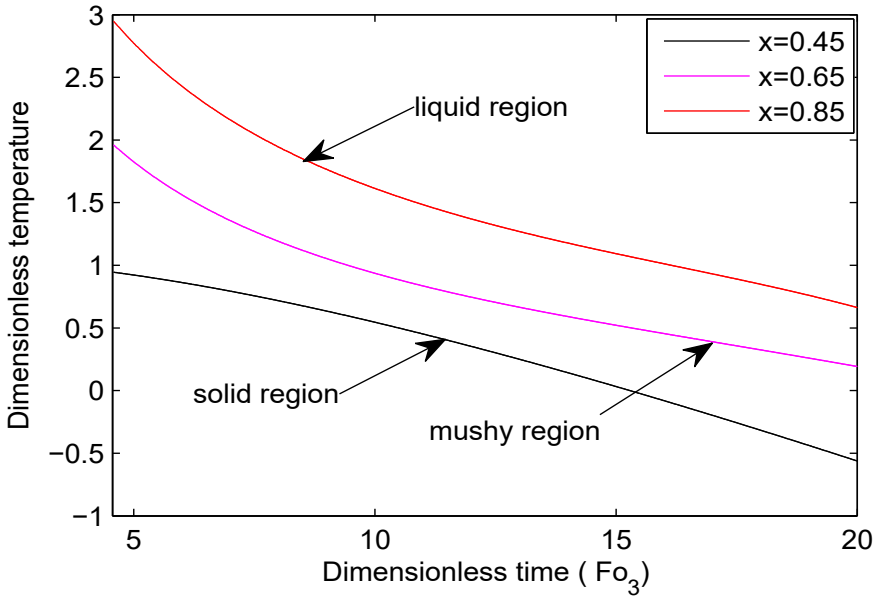

Figure 4.15: Dimensionless temperatures with time Fo_3 in stage 3 (2), $Pd_3 = 0.2177, \eta_1 = 0.002, \lambda_1 = 0.2573, \lambda_2 = 0.4729$.

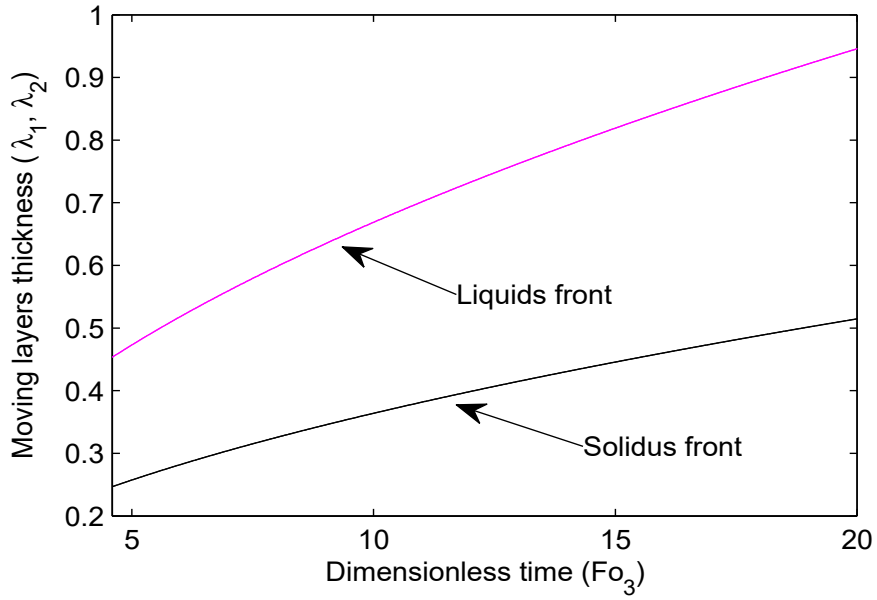

Figure 4.16: Moving layer thickness (λ_1, λ_2) with dimensionless time Fo_3 in stage 3 (2).

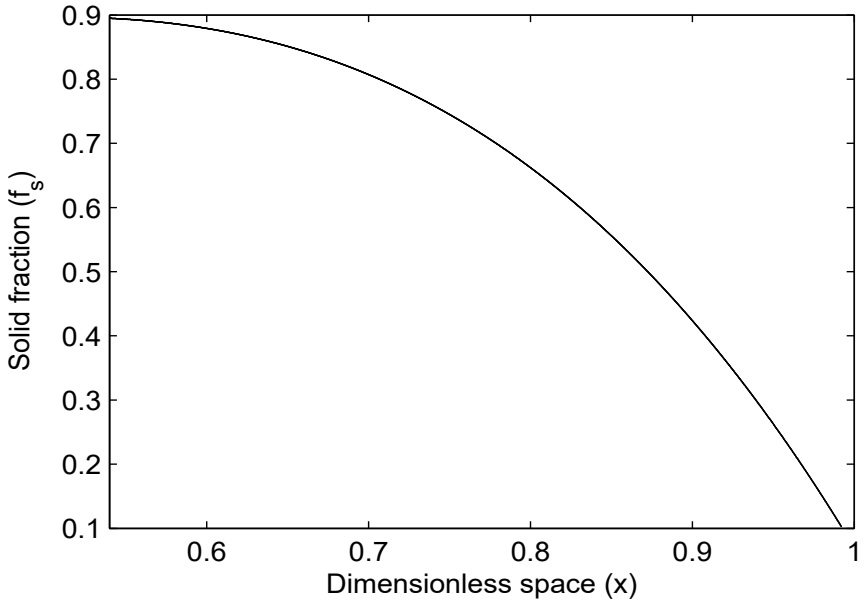

Figure 4.17: Solid fraction (f_s) in mushy zone with dimensionless space x in stage 3 (2), $Fo_3 = 22$.

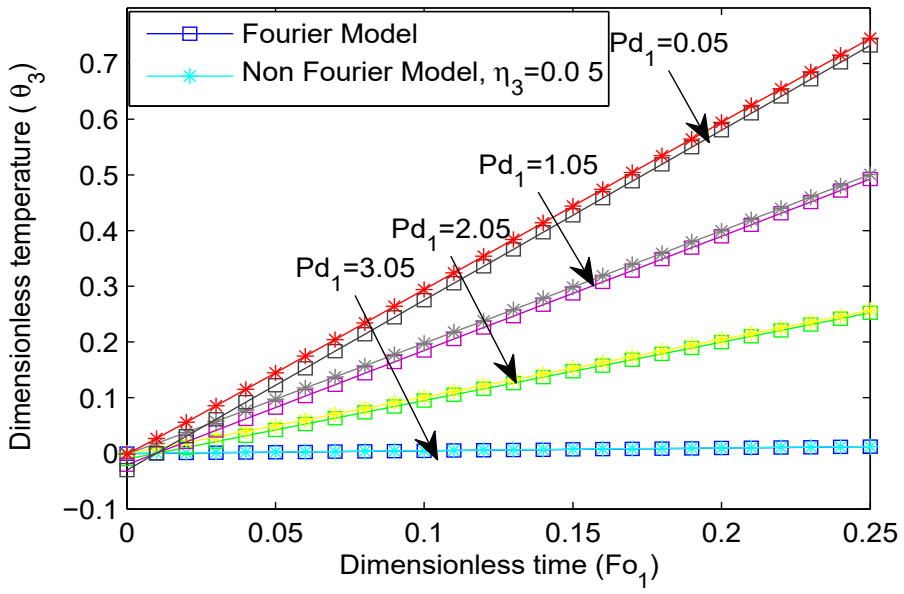

Figure 4.18: Effect of relaxation time on dimensionless temperatures θ_3 with dimensionless time Fo_1 in liquid region.

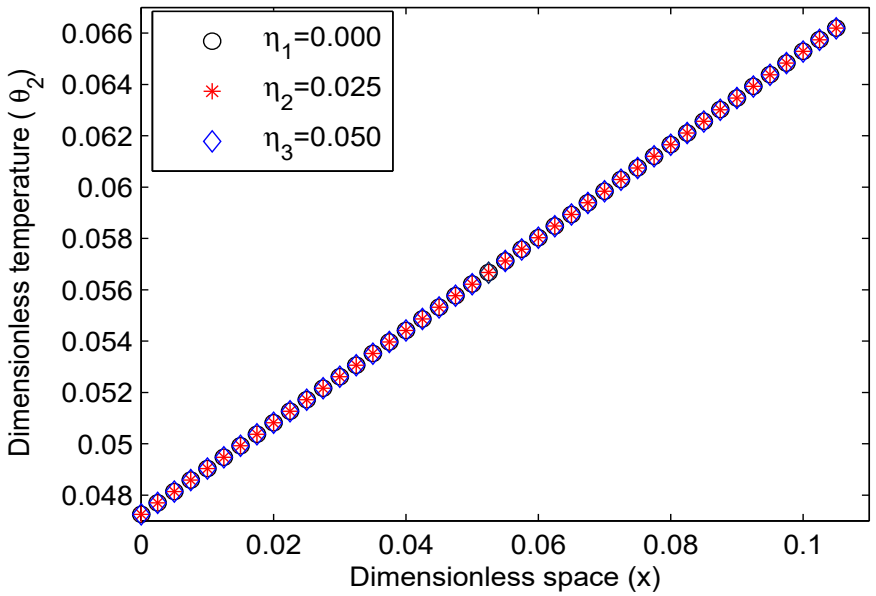

Figure 4.19: Effect of relaxation time on dimensionless temperatures θ_2 with dimensionless space x in mushy region.

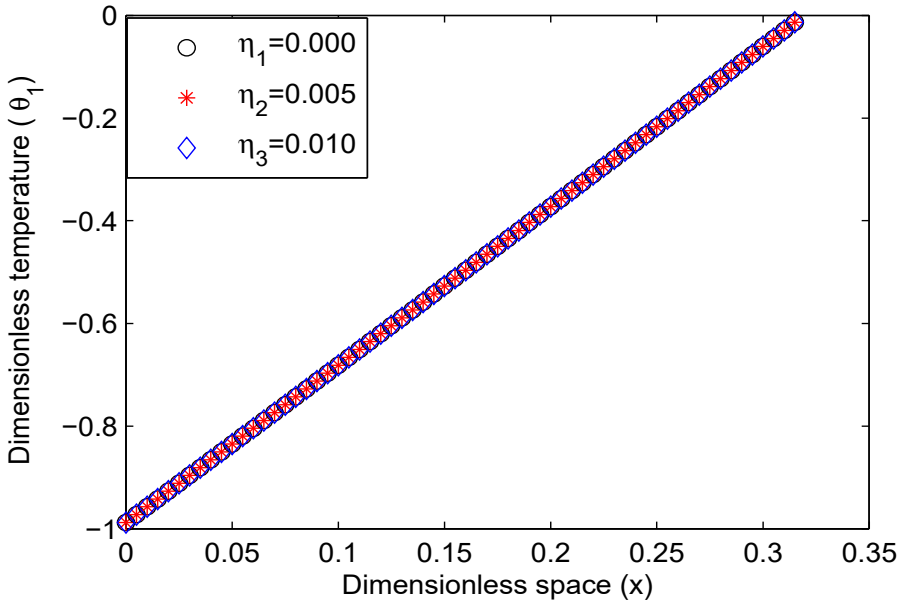

Figure 4.20: Effect of relaxation time on dimensionless temperatures θ_1 with time Fo_3 in solid region.

4.5 Conclusion

In this paper, we developed the time relaxation model for binary eutectic system. We have proved that our model is well posed. To solve this model we have developed the Legendre wavelets spectral Galerkin method and proved that the present method is stable. From our simulations we observed that, initially the solid fraction present in mushy region increases as space coordinate increases and after some times when solid starts to form the solid fraction present in mushy region decreases as space coordinate increases. The liquidus moving layer thickness moves fast as compare to solidus moving layer thickness. The effect of relaxation time is presented in liquid region and the effect of relaxation time present in mushy and solid region, is negligible. Further, we have compared the Fourier model with non-Fourier model, both the model coincide as Predvoditelev number (Pd_1) increases with time Fo_1. From Fig. (4.6), It has been noted that the temperature in liquid region continues to decrease with space while in Fig. (4.14) observation is reverse. This may be due to the two different models of f_{su}. Both the models appear to be relevant for industrial application through which compassion and components of melt can be predicted reasonably well. These mathematical models will very useful for experimental analysis of solidification process.